UC Berkeley
UC Berkeley Previously Published Works

Title
Surface origin and control of resonance Raman scattering and surface band gap in indium nitride

Permalink
https://escholarship.org/uc/item/3sq5f5hd

Journal
Journal of Physics D, 49(25)

ISSN
0022-3727

Authors
Alarcón-Lladó, Esther
Brazzini, Tommaso
Ager, Joel W

Publication Date
2016-06-29

DOI
10.1088/0022-3727/49/25/255102

Peer reviewed

eScholarship.org Powered by the California Digital Library
University of California

Surface origin and control of resonance Raman scattering and surface band gap in indium nitride

Esther Alarcón-Lladó,[1,2] **Tommaso Brazzini,**[2,3†] **and Joel W. Ager**[2,*]

[1]Swiss Federal Institute of Technology (EPFL), Lausanne, Switzerland

[2]Materials Sciences Division, Lawrence Berkeley National Laboratory, Berkeley, CA, USA

[3]Dep. Ingeniería Electrónica and Instituto de Sistemas Optoelectrónicos y Microtecnología, ETSI Telecomunicación, Universidad Politécnica de Madrid, 28040 Madrid, Spain

E-mail: JWAger@lbl.gov

[†]Current address: Center for Device Thermography and Reliability (CDTR), H.H. Wills Physics Laboratory, University of Bristol, Tyndall Avenue, Bristol BS8 1TL, United Kingdom

Abstract.

Resonance Raman scattering measurements were performed on indium nitride thin films under conditions where the surface electron concentration was controlled by an electrolyte gate. As the surface condition is tuned from electron depletion to accumulation, the spectral feature at the expected position of the (E_1,A_1) longitudinal optical (LO) near 590 cm^{-1} shifts to lower frequency. The shift is reversibly controlled with the applied gate potential, which clearly demonstrates the surface origin of this feature. The result is interpreted within the framework of a Martin double resonance, where the surface functions as a planar defect, allowing the scattering of long wavevector phonons. The allowed wavevector range, and hence the frequency, is modulated by the electron accumulation due to band gap narrowing. A surface band gap reduction of over 500 meV is estimated for the conditions of maximum electron accumulation. Under conditions of electron depletion, the full InN bandgap (E_g = 0.65) is expected at the surface. The drastic change in the surface band gap is expected to influence the transport properties of devices which utilize the surface electron accumulation layer.

1. Introduction

The origin of the intense peak appearing in the resonance Raman spectrum of wurtzite InN films in the vicinity of the expected (E_1,A_1) longitudinal optical (LO) frequency has been of considerable interest for the last decade. In contrast to GaAs and other III-V semiconductors, where the LO phonon couples to free carriers and forms coupled L^- and L^+ modes [1], the LO-like scattering in InN and in In-rich InGaN has only a small shift in frequency regardless of electron (hole) concentration [2,3]. A number of groups have attributed the LO-like feature observed in the $z(-,-)\bar{z}$ scattering geometry from *c*-axis oriented wurtzite InN films to an unscreened A_1(LO) mode with a large wavevector (q) [4,5]. The phonon is uncoupled from the typically large (degenerate) free electron densities due to the breakdown of the q-conservation. Some authors have attributed the wavevector non-conservation to the presence of bulk impurities.[6] However, this explanation appears to be inconsistent with Cusco *et al*. who confirmed the conservation of wavevector in the scattering process in bulk InN by the observation of the L^- phonon-plasmon coupled mode in a series of doped InN layers [7].

Recently, a double resonance mechanism was proposed by Davydov *et al*. to explain the presence of large-q phonons in the Raman spectra of InN [8]. The mechanism is based on the double resonance theory of Martin [9], and a strong dependence of the frequency of the LO modes on the excitation frequency is predicted and observed. A similarly strong dispersion of the LO-like scattering with excitation frequency was also observed in InN nanowires, providing further support for a double resonance mechanism [10]. However, this proposed scattering mechanism relies on elastic scattering of photoexcited carriers in the intermediate Raman state, which is attributed to the presence of impurities in the bulk material. Also, the LO-like scattering is assumed to have its origin in the bulk of the material.

There is recent evidence that the surface may play an important role in the Raman scattering of InN thin films. For example, Cho *et al*. have used cross-sectional Raman microscopy to observe a large increase in scattering from the surface of InN thin films [11]. Kranert *et al*. have proposed a model for wurtzite semiconductors in which wave-vector nonconservation can be caused, under resonant excitation conditions, by considering the surface as a planar defect [12].

In this work we critically examine the attribution of the LO-like scattering to the bulk of the InN films. InN is well-known to have a surface electron accumulation (SEA) layer with an areal density in the low-mid 10^{13} cm^{-2} range [13], regardless of the surface orientation [14,15]. The SEA

layer, which is depicted schematically in Fig. 1(a), extends over a range of ca. 10 nm given the range of electron (hole) concentrations observed in bulk of InN films (10^{17}-10^{19}, typically) [14,16]. While the presence of the SEA layer has prevented the realization of many traditional semiconductor device architectures, a number of InN-based devices have been demonstrated which utilize the SEA as a conducting channel. These include chemical and anion-sensitive sensors [17,18] and both electrolyte and dielectric-gated field effect transistors [19–21].

Here we employ electrolyte gating to control the electron concentration in the SEA with concurrent *in-situ* optical probing by means of Raman spectroscopy. We note that a conceptually similar approach has been used to investigate near-surface electronic Raman scattering in graphene using electrolyte gating [22,23] and in III-V semiconductors and silicon using metal-insulator-semiconductor structures [24,25]. We provide definite proof of the surface origin nature of the controversial LO-like Raman scattering in InN. We find that the LO-like Raman feature is reversibly modulated with gate voltage and follows a universal behavior regardless of the bulk doping properties. The shifts of this peak with changes in the surface electron concentration are consistent with a Martin double resonance mechanism, in which larger phonon wavevectors become accessible under electron accumulation conditions due to band gap narrowing. We believe that the surface acts as mediator for the double resonance scattering process, contrary to what has been believed up to now. Moreover, the surface band gap narrowing should substantially influence the electron transport in SEA devices based on InN, and possibility, other small band gap semiconductors.

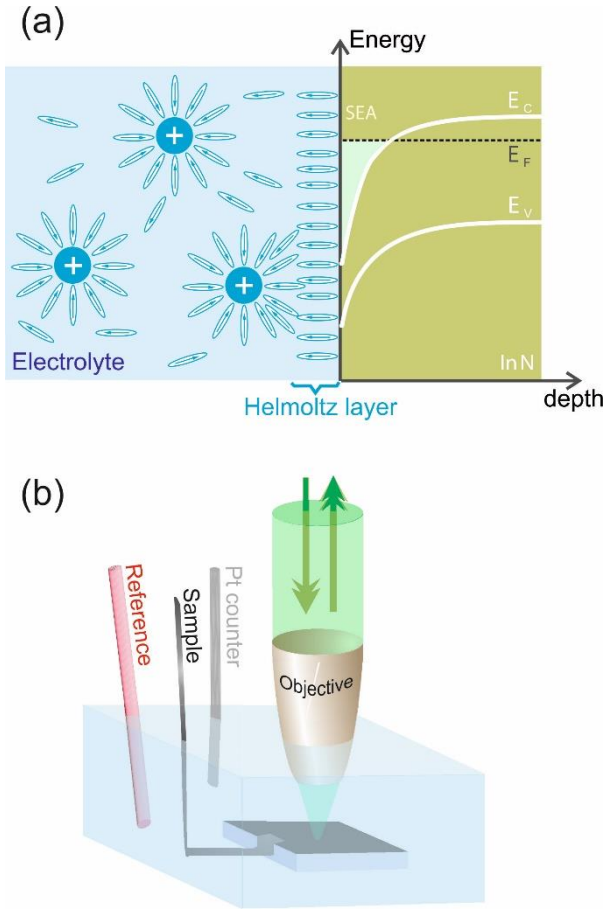

Figure 1. (color online) Surface electron accumulation and experimental configuration. In (a) the surface band bending of InN is depicted for a sample with a non degenerate *n*-type bulk doping behavior. The surface Fermi level is pinned above the conduction band minimum (E_C), resulting in a surface electron accumulation (SEA) layer. The Helmholtz double layer which forms at the electrolyte/InN interface allows bias to be applied to the InN to either further accumulate or deplete the SEA. The optical measurement setup is shown in (b). Bias was applied to the InN with respect to the reference electrode using a standard 3-electrode configuration being controlled by a potentiostat. The microscope objective used to excite the InN surface and collect Raman scattered light was immersed in the electrolyte. It was chemically and electrically insulated from the electrolyte by a thin sheet of Teflon.

2. Experimental

InN thin films used in this study were grown by molecular beam epitaxy (MBE) on GaN templates. All films are *c*-axis oriented and have the wurtzite structure. Mg doping was used to produce p-type films,[26,27] while the *n*-type film was not intentionally doped. Details of the growth method and of the electrical characterization are reported elsewhere.[27] The samples were chosen to represent the range of n- and p-type InN available with MBE growth. The transport properties of the films used in this study are shown in Table 1.

Table 1. Structural and electrical transport properties of the InN films used in this study. The thickness (t) of the main InN layer excluding the buffer and the results of Hall (n_e, μ_e) and Seebeck (S) measurements are shown. Hall measurements for the 3 Mg-doped samples reflect electron transport in the accumulation layer only;[26] it is not possible to measure the hole concentration and mobility in the bulk of the film using this technique.[27] The positive value of the Seebeck coefficient for P2 and P3 confirms that the bulk of these films is p-type.[26] P1 is Mg doped but at a level below that of compensating donors, resulting in an overall negative Seebeck coefficient.

Sample	Film/buffer/template	t (nm)	n_e (10^{18} cm^{-3})	μ_e (cm^2/V s)	S (μV/K)
N1	InN/GaN	500	2.7	1025	-111(n)
P1	InN:Mg/60nm-InN/GaN	500	-	-	-167(n)
P2	InN:Mg/10nm-InN/ GaN	1000	-	-	+50(p)
P3	InN:Mg/10nm-InN/GaN	2000	-	-	+270(p)

The optical and electrical measurement setup is shown in Fig. 1(b). Raman microprobe spectra were recorded at room temperature in the $z(-,-)\bar{z}$ scattering geometry. Laser excitation was provided either by a He-Ne (1.96 eV) or diode laser (2.33 eV) and the scattered light was collected by an optical microscope and was analyzed with a Jobin-Yvon LabRAM-HR spectrometer. A 0.5 M NaOH solution was used as the liquid electrolyte and a Biologic potentiostat was used to control the bias applied to the surfaces of the film. A water immersion objective (x64) was used to focus the incident laser beam and collect the scattered light. It was chemically and electrically insulated from the electrolyte by a thin Teflon sheet [28]. The reference electrode was either Ag/AgCl or Hg/HgO and a platinum wire was used as the counter electrode. The sample potential was measured with respect to the reference electrode and is reported versus the normal hydrogen electrode (NHE). The surface of the InN thin films were HCl etched prior to the experiments in order to remove any surface oxides. Indium was used as ohmic contact to InN and was protected from the electrolyte by chemically resistant epoxy. The gate voltage was varied only in the regime in which there was negligible current flow between the InN and the electrolyte to prevent electrochemical reactions and/or etching of the film, both in the dark and under laser illumination.

We have shown previously that the insulating double layer which forms when a conformal liquid electrolyte is in contact with the surface of InN (Fig. 1(a)) allows bias potentials to be applied under conditions of minimal current flow. The electron concentration in the SEA in thin films can be increased, decreased to the bulk value (at the flat band potential), and even inverted to hole accumulation [29–31]. For the geometry employed here, more positive bias will deplete the

surface while more negative bias will increase the electron accumulation. As we observed the largest effects in accumulation (see below), we will concentrate on changes caused by increasing the SEA with negative bias voltages.

3. Results

Capacitance-voltage (C-V) measurements were performed to determine the flat-band potential of the thin film samples, as shown in Fig. 2(a). In InN surface donors, ionized bulk donors/acceptors, and surface holes due to inversion at large positive biases all contribute to the observed capacitive space charge. As a result, the C-V data do not follow a simple linear relationship when graphed in the Mott-Schottky (C^{-2} vs. V) form. Instead, quantitative analysis of C-V data results requires solving the Poisson equation to determine the near surface electron concentration as a function of bias.[16,29] Here, the 1D Poisson equation was solved by using the *nextnano*[3] software (copyright ©2012, nextnano GmbH, Germany). The surface Fermi level pinning was taken into consideration by using a Schottky barrier of 650mV at the InN surface. An ohmic back contact was used as the second boundary condition. The simulation allow the space charge density to be calculated as a function of applied voltage. At 0 V, the sheet electron density is between 10^{13} and 10^{14} cm^{-2}, depending on doping, which is in agreement with experimental literature reports [13,14,30,32]. Then, the capacitance was calculated from the derivative of the charge density as a function of voltage. A shift of 0.2 V was considered to account for the difference between the InN surface in air and water. The shift is taken from the difference between optical experiments in air and under water, described below. The C^{-2} vs. V modeling results are shown as solid lines in Fig 2(a). The good agreement of the model with the experimental data allows us to rule out any effects due to incorporation of ions into the near surface region. The doping densities used for the simulations are labeled in the figure. We find that the flat band potential for the *n*-type sample is ~0.35 V vs. NHE, while for *p*-type samples the flat band potentials are ca. 1 V vs. NHE, with the difference corresponding approximately to the band gap of InN. The increase in slope of the C^{-2} vs. V data with increasing positive bias reflects the change in contribution to the capacitance from the SEA to the space charge region in the bulk defined by the bulk doping as the surface condition is tuned from accumulation to depletion [16].

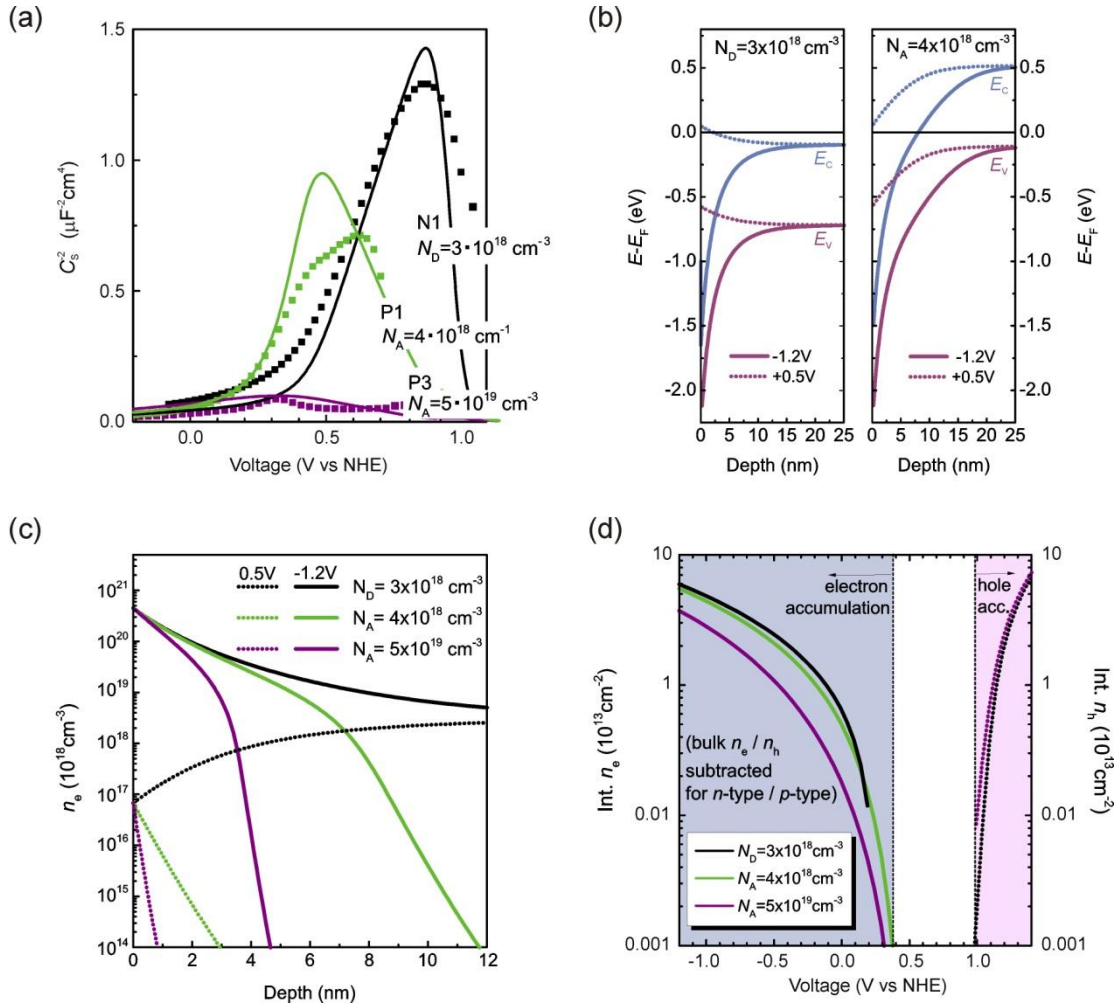

Figure 2. (color online) (a) $1/C^2$ as a function of applied voltage to the semiconductor determined by electrochemical capacitance-voltage (ECV) measurements for differently doped InN samples used in this work along with three calculated curves for N_D=3x10^{18} cm^{-3}, N_A=4x10^{18} cm^{-3} and N_A=5x10^{19} cm^{-3}. The measurements were performed at 1 kHz with 0.5M NaOH solution as the electrolyte. Calculated lines were obtained by solving the Poisson equation. (b) Band bending under strong (solid lines) and moderate (dashed lines) accumulation conditions for two bulk doping values; degenerate *n*-type and non-degenerate *p*-type (c) Calculated electron concentrations for the strong and moderate accumulation conditions (d) Calculated integral electron density as a function of voltage for the same acceptor/donor bulk densities as in (a). The contribution from the bulk has been subtracted for clarity. Shaded blue (red) areas indicate the voltage region for which electrons (holes) are accumulated at the surface.

The solution to the Poisson equation also allows assessing the changes in band energy profiles as a function of voltage. Fig 2(b) shows the modulation given by the gate voltage to the InN surface band structure based on the assumed values in the capacitance-voltage simulations. Two doping conditions are plotted (N_D=3 10^{18}cm^{-3} and N_A=4 10^{18} cm^{-3}). The near-surface band bending was calculated for InN under two different voltages (V=-1.2 and +0.5V vs NHE), which represent a strong and moderate electron accumulation conditions. As can be observed, the band bending, and thus the electric field, strongly depends on the bulk doping concentration as well as gate voltage.

Fig 2(c) shows the depth profile of the electron concentration for the same voltage inputs and bulk doping conditions. Although the depth profile of n_e strongly depends on bulk doping, the integrated sheet electron/hole accumulation (subtracting the bulk value) still remains rather similar for a large range of bulk concentrations and gate voltages (Fig 2(d)). In essence, over the range of potentials (-1 to +0.8 V vs. NHE) which will be employed in the *in-situ* Raman experiments described below, the sheet carrier density in the SEA is modulated from $<10^{11}$ to $>10^{13}$ cm^{-2}, according to our calculations.

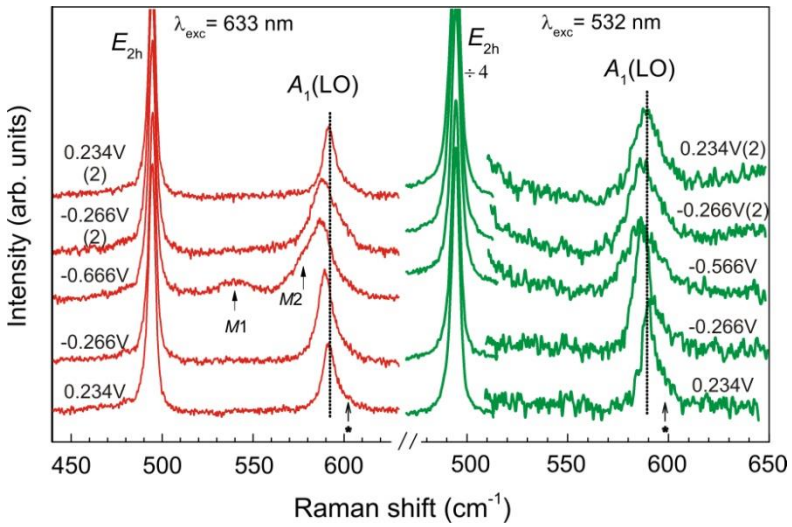

Figure 3. (color online) Raman spectra of *n*-InN (sample N1 in this manuscript) at 0 V and at negative voltage (accumulation conditions) *vs* NHE with 633 nm (left) and 532 nm (right) excitation wavelengths. Spectra have been normalized to the E_{2h} intensity and are vertically shifted for clarity. The dotted vertical line indicates the position of the LO mode at 0.234 V vs NHE. The voltage has been swept from 0.234 to -0.666V and back to 0.234V vs NHE in order to show the reversibility of the effect (the order of the spectra is bottom to top). The DALO band is marked with an asterisk (see text).

Figure 3 shows the *in-situ* Raman spectra as a function of bias from sample N1. In this backscattering geometry, the non-polar E_{2h} mode and the A_1(LO) mode are allowed by symmetry [12]. Spectra are normalized to the height of the E_{2h} phonon. As reported in many earlier works, the A_1(LO) peak is relatively more intense under red light excitation, indicating near resonance conditions, in spite of the large difference between the excitation energy (1.96 eV) and band gap of InN (0.69eV) [33]. At a first glance, one can see that, regardless of excitation energy, the frequency of the LO-like scattering near 590 cm^{-1} shifts to lower frequency as the electron accumulation is increased by applying a negative bias (gate changed from around +0.2 to -0.6V vs NHE), while the E_{2h} peak is unchanged. This effect is completely reversible and the peak position returns to its original position when the potential is returned to above 0.2 V vs. NHE. The reversible shift of the LO-like feature with gate voltage was observed in all samples studied

regardless of the bulk doping condition. Figure 4 shows exemplary spectra from all other samples which illustrate this point. Apart from the LO mode shift and broadening, which is common in all samples, there are more subtle changes in the spectra which occur under strong electron accumulation conditions. Close examination of the spectra in Fig. 3 and 4 show that a new peak (*M1*, at ~540 cm^{-1}) and a shoulder on the LO phonon (*M*2) appear under resonance conditions (633 nm wavelength). The possible origin of these modes will be discussed below.

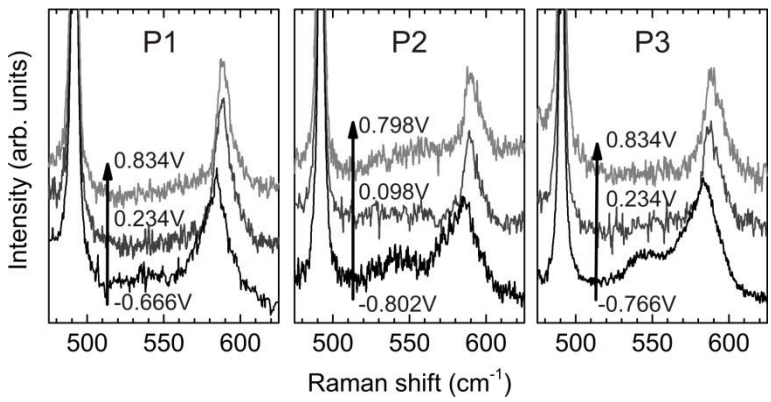

Fig. 4 Raman spectra of Mg-doped InN (samples P1 to P3) at negative, 0V and positive voltage *vs* NHE. Spectra have been taken under red light excitation conditions. All spectra have been normalized to the E_{2h} intensity and are vertically shifted for clarity.

In order to quantify changes in the LO peak as a function of voltage, we fit the spectra to Lorentzian lineshapes. In most cases, a weak disorder–activated longitudinal (DALO) band was included as a high frequency shoulder (marked with an asterisk in Fig. 3), and for the red-excited spectra, a third peak (*M*2) has been taken into account for the deconvolution. We also corrected the peak frequencies of all features for strain caused by the heteroepitaxial growth using the difference in E_{2h} frequency with respect to the reported unstrained value of 491.5 cm^{-1} (refs. **Error! Bookmark not defined.** and **Error! Bookmark not defined.**) and using the values for the relationship between the frequency shift and strain ($\Delta\omega/\Delta\sigma_a$) for the E_{2h} and A_1(LO) modes of –9 cm^{-1}/GPa and –8.4cm^{-1}/GPa, respectively [34], where σ_a is the biaxial stress and $\Delta\omega$ is the strain-induced shift. Figure 5(a) summarizes the shift of the LO phonon as a function of bias for all thin films samples. The FWHM of the main LO peak is shown as a function of bias in Fig 5(b). Figure 5 shows that the changes in the LO phonon scattering produced by electrolyte gating are large: the peak frequency red shifts by up to ~6 cm^{-1} and its FWHM increases by nearly a factor of two under accumulation conditions. It is also clear that the *n*-type and the three Mg-doped samples show a universal behavior, within our experimental resolution, in terms of the accumulation-induced red-shift and broadening of the LO phonon feature for both laser excitation wavelengths.

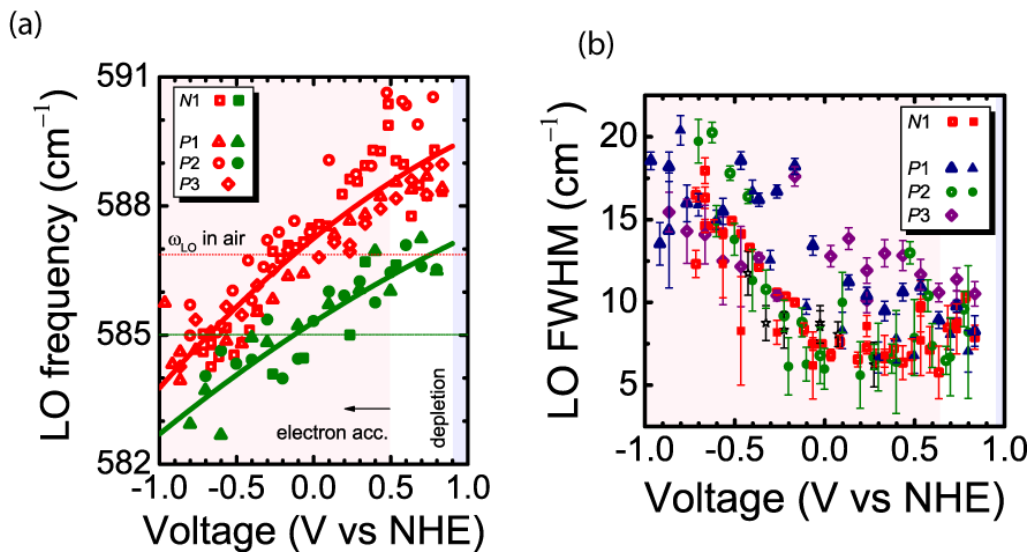

Fig. 5 (color online) (a) Frequency of the longitudinal optical Raman peak (strain corrected) for the differently doped InN samples as a function of voltage. Empty (filled) data points were obtained by using the 632.8 nm (532 nm) excitation line. The red dotted (green dashed) line corresponds to the frequency of the LO mode of InN in air probed by 632.8nm (532 nm) laser line. The red (blue) shadowed area indicates the voltage range for which electrons (holes) are being accumulated at the surface (b) Voltage dependence of the LO peak FWHM.

4. Discussion

We begin with a discussion of the LO phonon scattering and how it is affected by gate voltage. As shown in Fig 2(b)-(c), electrolyte gating produces changes in the electron concentration in only the top ca. 10 nm of the InN films. Thus, the observation that the A_1(LO) Raman peak shifts controllably and reversibly with the applied potential clearly demonstrates the surface origin of this feature. As seen in Fig. 5(a), the frequency trend of the LO mode is the same for all four of the InN samples studied in this work and for both laser excitations: the more negative the voltage, i.e. the more electron accumulation, the lower the LO frequency.

The dotted red and green horizontal lines in Fig. 5(a) indicate the frequency position of the A_1(LO) peak in air. As mentioned above, the frequency in air is obtained again under electrolyte controlled conditions at -0.2 V vs NHE, indicating a slight depletion effect created by the water electrolyte immersion. The A_1(LO) frequency in air is about 2 cm^{-1} larger for red excitation compared to green in agreement with the study of Davydov *et al.*[8] In that study, it was proposed that Martin's double resonance is responsible for the observation of A_1(LO) with large values of the phonon wavevector q.[8] In their work, they observe a red-shift of the LO phonon with increasing the excitation energy, consistent with the prediction that the phonon wavevector (q_{ph}) can be twice that of the photoexcited electron-hole (k_{eh}), as shown schematically in Fig. 6. Thus, an increase in the above bandgap excitation energy will allow electrons to be promoted to the

conduction band at larger k_{eh}, and in turn are able to scatter LO phonons of larger q_{ph}. Our observation of a larger ω_0 for red vs. green excitation is clearly consistent with this mechanism.

The present work clearly demonstrates the surface nature of the LO feature, given by the ability to tune its frequency through modulating the electron concentration at the surface. Kranert *et al.*, have recently proposed a model in which surface defects can lead to the wavevector non-conservation required for large q_{ph} to be observed in wurtzite material [12]. The fact that the surface can act as a planar defect, allowing the 1LO resonant mode to be scattered, can explain both the presence of Martin's double resonance in high quality InN and our findings. Regarding the large frequency shift produced by tuning the gate voltage, we are evidently probing A_1(LO) with different q_z across the Brillouin zone. Calculations of the phonon dispersion in wurtzite InN of the A_1(LO) dispersion from the Γ point to the A point predict a red-shift of 8-10 cm^{-1} across the width of the zone [8,35]. Considering both laser excitations, the data shown in Fig. 5(a), in which the electrolyte gating tunes the A_1(LO) frequency from ~590 cm^{-1} (red excitation, depletion) to ~583 cm^{-1} (green excitation), suggests that a wide range of q is being accessed. We will explain this effect by a combination of a Martin double resonance, the surface origin of the momentum non-conversation, and an SEA-induced change in the surface band structure.

It is known that high electron concentrations reduce the band gap, both in the bulk [36] and in 2D structures [37,38]. Thus, it would be expected that the band gap near the surface of InN would be reduced as compared to the bulk as a result of the electron accumulation. Indeed, this effect has been quantified experimentally for InN by angle resolved photoemission by King *et al.*[39] Remarkably, for InN samples in vacuum, the surface band gap was reduced by 450 meV compared to the bulk value (690 meV). For our work, we expect a similar reduction in the surface band gap in air and an even larger reduction by increasing the SEA through gating.

It is possible to estimate the range of q accessible by the laser excitation energies we used and with the magnitudes of $n_{surface}$ available by electrolyte gating shown in Fig. 2(c)-(d). It is known that the band gap shrinkage scales with $(n_{surface})^{1/3}$, as has been experimentally predicted and observed in many systems [37,38,40]. In the work by King *et al.*, the 2D carrier density was ~1.6x10^{13} cm^{-2} before renormalization. This corresponds to an electron concentration at the surface of ~2x10^{20}cm^{-3}, according to our calculations as described above. Using the reported band gap reduction of 450meV, we obtain

$$\Delta E_g \approx -7.69\ 10^{-5}\ \text{meV cm}\ (n_{surface})^{1/3}. \quad (1)$$

Referring to Figs. 2(b)-(d) and to Eq. (1), we estimate a bandgap reduction of ~550 meV for the largest negative potential used in this study (V=-1V vs NHE). Similarly, the full InN bandgap (ΔE_g = 0) at the surface is expected for a voltage of +0.6V vs NHE and above.

We used 8x8 *k-p* theory to apportion the band gap reduction between the conduction and valence bands.[41,42] For the scattering results discussed here, with the surface acting as a planar defect allowing the transfer of momentum from the photoexcited charge to the lattice, along the [0001] direction. In this direction, the light holes and heavy holes in InN have a similar effective mass, about $1.56m_e$.[43] Lighter holes are found at the split-off band with an effective mass of $0.12m_e$. In the 8x8 *k-p* analysis, which is performed for $k_x = k_y = 0$ and $k = k_z$, we include the crystal field splitting, spin orbit interaction and band gap reduction. The band dispersions is found by diagonalizing the following Hamiltonian:

$$H_{8x8} = \begin{pmatrix} Ec + \frac{\hbar^2 k^2}{2\,m_e} & 0 & 0 & k\,P & 0 & 0 & 0 & 0 \\ 0 & \mathrm{F} + \frac{\Delta_{\mathrm{SO}}}{3} & 0 & 0 & 0 & 0 & 0 & 0 \\ 0 & 0 & \mathrm{F} - \frac{\Delta_{\mathrm{SO}}}{3} & 0 & 0 & 0 & 0 & \frac{\sqrt{2}}{3}\Delta_{\mathrm{SO}} \\ k\,P & 0 & 0 & \lambda & 0 & 0 & \frac{\sqrt{2}}{3}\Delta_{\mathrm{SO}} & 0 \\ 0 & 0 & 0 & 0 & Ec + \frac{\hbar^2 k^2}{2\,m_e} & 0 & 0 & k\,P \\ 0 & 0 & 0 & 0 & 0 & \mathrm{F} + \frac{\Delta_{\mathrm{SO}}}{3} & 0 & 0 \\ 0 & 0 & 0 & \frac{\sqrt{2}}{3}\Delta_{\mathrm{SO}} & 0 & 0 & \mathrm{F} - \frac{\Delta_{\mathrm{SO}}}{3} & 0 \\ 0 & 0 & \frac{\sqrt{2}}{3}\Delta_{\mathrm{SO}} & 0 & k\,P & 0 & 0 & \lambda \end{pmatrix}, \quad (2)$$

where

$$E_C = E_g + \Delta_{\mathrm{CF}} + \frac{1}{3}\Delta_{\mathrm{SO}}, \quad (3a)$$

$$F = \Delta_{\mathrm{CF}} + \lambda + \theta, \quad (3b)$$

$$\lambda(k) = \frac{\hbar^2 k^2}{m_0} A_1, \text{ and} \quad (3c)$$

$$\theta(\mathrm{k}) = \frac{\hbar^2 k^2}{m_0} A_3. \quad (3d)$$

P is the Kane parameter (0.757 eV nm), Δ_{CF}= 40 meV, Δ_{SO}= 5 meV, and E_g = 0.69 eV +ΔE_g where ΔE_g is calculated from Eq (1). A_i are valence band parameters defined as follows:

$$m_{hh}^* = -m_0(A_1 + A_3)^{-1} \text{ and} \quad (4a)$$

$$m_{ch}^{*} = -m_0\left(A_1 + \frac{E_{ch}^0}{E_{ch}^0 - E_{lh}^0}A_3\right)^{-1}, \text{ where} \tag{4b}$$

$$E_{ch}^0 = \frac{3\Delta_{\mathrm{CF}} - \Delta_{\mathrm{SO}}}{6} - \frac{1}{2}\sqrt{{\Delta_{\mathrm{CF}}}^2 + {\Delta_{\mathrm{SO}}}^2 - \frac{2}{3}\Delta_{\mathrm{SO}}\Delta_{\mathrm{CF}}} \text{ and} \tag{4c}$$

$$E_{lh}^0 = \frac{3\Delta_{\mathrm{CF}} - \Delta_{\mathrm{SO}}}{6} + \frac{1}{2}\sqrt{{\Delta_{\mathrm{CF}}}^2 + {\Delta_{\mathrm{SO}}}^2 - \frac{2}{3}\Delta_{\mathrm{SO}}\Delta_{\mathrm{CF}}}\,. \tag{4d}$$

To obtain m_{hh}^{*}=1.56m_e , and m_{so}^{*} = 0.12 m_e at the valence band maximum, A_1 = -8.36 and A_3 = 7.72. An approximation for small wavevectors was used by Davydov *et al*., where a 2-band interaction between the lightest holes and the conduction band was considered, with a non-interacting heavy hole band [8].

Figure 6 shows the evolution of the band structure and electron dispersion perpendicular to the surface as the condition is changed from flat-band (no accumulation) to strongly accumulated (from 0 to 550 meV in band gap reduction, Eq. (2)). It is clear that not only the band gap energy decreases with electron accumulation, but also the band edges become sharper resembling those of graphene. In each case, a Martin's double resonance scattering is also shown schematically, where the surface is responsible for the wave-vector non-conservation along the *z*-direction [12].

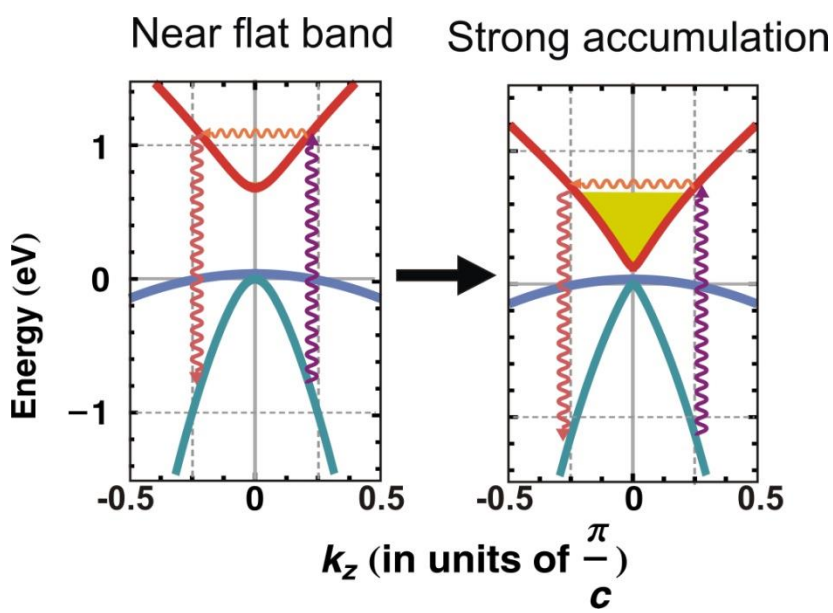

Figure 6 (color on-line). Schematic diagram of the proposed scattering mechanism as a function of band gap renormalization. The dispersion is given for wavevectors along the [0001] direction (i.e. along the $\Gamma - A$ line). The excitation energy is 1.96 eV. The surface allows elastic scattering of the exciton to give rise to long-wavevector phonons with q_{ph}=2k_z (horizontal arrows). Only optical transitions from the split-off to the conduction band are shown (see text).

By considering the band bending simulations shown in Fig. 2, along with Eqs (1) and (2), we estimate that the phonon wavevector q_{ph} range that is accessed by electrolyte gating ranges from

0.452 to 0.52 (in units of π/c_0) and from 0.538 to 0.606 (in units of π/c_0), for the red and green light excitations, respectively. This means, that by applying a gate voltage to our InN films, phonons within the second half of the BZ along the Γ-*A* direction are sampled, where the more negative voltages produce scattering from phonons the closer to the zone edge. These values were obtained by considering only the split-off band. For heavy holes, the q_{ph} resides outside the Brillouin zone (BZ). Moreover, as we observe a smooth trend of the experimental phonon frequency with voltage, we do not believe that resonances involving other bands make a large contribution to the scattering.

In order to correlate these findings with the experimental results, we use the LO phonon dispersion to find the frequency range accessed by surface gating. By taking the dispersion given in Ref. **Error! Bookmark not defined.** we find that for going from flat band to strong surface accumulation, the LO phonon should shift from 585.7 to 583.5 cm^{-1} for the red light excitation. For green light excitation, the predicted frequency range is from 583.0 to 580.6 cm^{-1}. In both cases, the experimental shift is in the same direction as the model, but the observed shift is somewhat larger (4-5.5 vs. 2-2.4 cm^{-1}, for red and green excitations respectively). We note, however, that there are uncertainties in both the effective mass parameters and phonon dispersion for InN, which may explain some of the discrepancy. It is also possible that the large electric field produced by the strong surface band bending plays a role.

Now, we turn to the origin of the broadening under strong electron accumulation, Fig. 5(b). We note that the maximum line widths observed, ca. 20 cm^{-1}, are larger than the predicted maximum dispersion of the A_1(LO) phonon from zone center to edge. We believe that the phonon lifetime is decreased under strong electron accumulation conditions, which will cause additional Raman line broadening.

Finally, we want to address the observation of the two peaks (labeled *M*1 and *M*2 in Fig. 3) that are observed for negatively gated InN. The feature *M*1 is the most clear and appears at a frequency of around 540 cm^{-1}. We note that the frequency is very close to that of the forbidden B_{1h} silent mode which has been observed experimentally in the near surface region by second harmonic generation spectroscopy [44]. *M*2 is a shoulder on the LO feature at about 585 cm^{-1}. The observation of Raman peaks around the frequencies of *M*1 and *M*2 have been reported in other studies [5,45–49]. While some attribute it to the B_1 silent mode arising from sample imperfections, others have assigned them to surface optical (SO) modes with A_1 and E_1 symmetries. Interestingly,

Schäfer-Nolte *et al*. suspected that these peaks appearing in highly doped samples could be related to electron transitions at localized states [46]. In our work, we see that both features are clearly enhanced by long wavelength excitation and the presence of large electron densities at the surface, which follows the theory of electron-related transitions. Figure 7 shows the intensity trend of these two features as a function of applied voltage. It is clear from the identical exponential increase in intensity of *M*1 and *M*2, regardless of sample nature, that there is a direct link between carrier density and/or band structure at the surface and these Raman features.

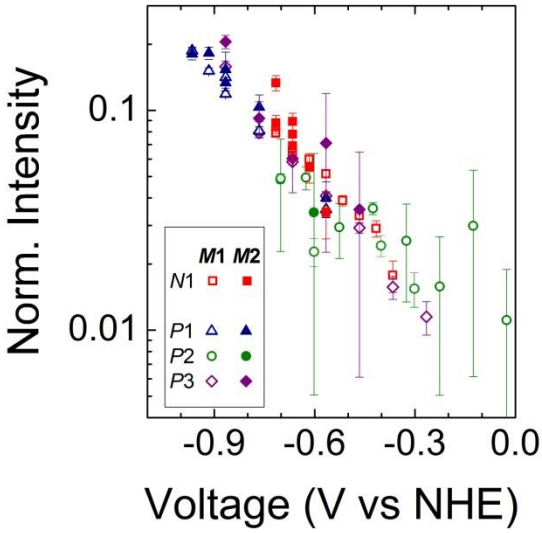

Figure 7 (color on-line). Normalized intensity of features M1 and M2 (see Fig. 3(a)) as a function of bias. Normalization is performed with respect to the E_{2h} mode. The y-axis is in logarithmic scale.

5. Conclusions

In-situ micro-Raman measurements were used to probe directly the interaction between the surface electron accumulation layer and the Raman-active phonons. We find that the intensity and frequency of the forbidden LO Raman feature is reversibly changed by the external potential, showing its surface. This is the first experimental evidence of the relation between the LO feature in InN and free electron accumulation at its surface. Martin's double resonance mechanism is responsible for long-wavelength LO scattering at the InN surface. By changing the band bending at the surface, both carrier density and band structure are modulated, which in turn changes range of LO phonon wavevectors which contribute to the scattering.

The changes in the surface band structure produced by controlling the SEA are significant. Under condition of maximum accumulation, the surface band gap is predicted to be reduced from its bulk value of 0.65 eV by over 0.5 eV and our 8x8 *k-p* analysis predicts that the band edges should become very sharp, resembling those of graphene. This would be expected to have a large

influence on the electron transport in the SEA. Under condition of electron depletion, the surface band gap should be similar to the bulk value.

6. Acknowledgments

This work was supported by Director, Office of Science, Office of Basic Energy Sciences, Materials Sciences and Engineering Division, of the U.S. Department of Energy under Contract No. DE-AC02-05CH11231. EAL acknowledges the support from the Marie Curie Actions. TB acknowledges the support by the EU under the Grant Agreement No. PITN-GA-2008-213238, Initial training network RAINBOW of the 7 RTD Framework. We thank Alex Bell, Jason Yeo Boon Siang and Mary Louie for the use of their Raman microprobe instruments. We also thank Jordi Ibáñez Insa for fruitful discussions.

7. References

[1] Cardona M and Guntherodt G 1984 *Light Scattering in Solids IV* (Springer Berlin Heidelberg)

[2] Davydov V Y, Emtsev V V, Goncharuk I N, Smirnov A N, Petrikov V D, Mamutin V V, Vekshin V A, Ivanov S V, Smirnov M B and Inushima T 1999 *Appl. Phys. Lett.* **75** 3297

[3] Ager J W, Walukiewicz W, Shan W, Yu K M, Li S X, Haller E E, Lu H and Schaff W J 2005 *Phys. Rev. B* **72** 155204

[4] Kasic A, Schubert M, Saito Y, Nanishi Y and Wagner G 2002 *Phys. Rev. B* **65** 115206

[5] Thakur J S, Haddad D, Naik V M, Naik R, Auner G W, Lu H and Schaff W J 2005 *Phys. Rev. B* **71** 115203

[6] Demangeot F, Pinquier C, Frandon J, Gaio M, Briot O, Maleyre B, Ruffenach S and Gil B 2005 *Phys. Rev. B* **71** 104305

[7] Cuscó R, Ibáñez J, Alarcón-Lladó E, Artús L, Yamaguchi T and Nanishi Y 2009 *Phys. Rev. B* **80** 155204

[8] Davydov V Y, Klochikhin A A, Smirnov A N, Strashkova I Y, Krylov A S, Lu H, Schaff W J, Lee H-M, Hong Y-L and Gwo S 2009 *Phys. Rev. B* **80** 81204

[9] Martin R 1974 *Phys. Rev. B* **10** 2620

[10] Domènech-Amador N, Cuscó R, Calarco R, Yamaguchi T, Nanishi Y and Artús L 2012 *Phys. Status Solidi - Rapid Res. Lett.* **6** 160

[11] Cho Y, Ramsteiner M and Brandt O 2013 *Appl. Phys. Lett.* **102** 72101

[12] Kranert C, Schmidt-Grund R and Grundmann M 2013 *New J. Phys.* **15** 113048

[13] Colakerol L, Veal T, Jeong H-K, Plucinski L, DeMasi A, Learmonth T, Glans P-A, Wang S, Zhang Y, Piper L, Jefferson P, Fedorov A, Chen T-C, Moustakas T, McConville C and Smith K 2006 *Phys. Rev. Lett.* **97** 237601

[14] Mahboob I, Veal T D, McConville C F, Lu H and Schaff W J 2004 *Phys. Rev. Lett.* **92** 36804

[15] King P D C, Veal T D, McConville C F, Fuchs F, Furthmüller J, Bechstedt F, Schley P, Goldhahn R, Schörmann J, As D J, Lischka K, Muto D, Naoi H, Nanishi Y, Lu H and Schaff W J 2007 *Appl. Phys. Lett.* **91** 92101

[16] Yim J W L, Jones R E, Yu K M, Ager J W, Walukiewicz W, Schaff W J and Wu J 2007 *Phys. Rev. B* **76** 41303

[17] Lu H, Schaff W J and Eastman L F 2004 *J. Appl. Phys.* **96** 3577

[18] Lu Y-S, Huang C-C, Yeh J A, Chen C-F and Gwo S 2007 *Appl. Phys. Lett.* **91** 202109

[19] Lin Y-S, Koa S-H, Chan C-Y, Hsu S S H, Lee H-M and Gwo S 2007 *Appl. Phys. Lett.* **90** 142111

[20] Lu Y-S, Chang Y-H, Hong Y-L, Lee H-M, Gwo S and Yeh J A 2009 *Appl. Phys. Lett.* **95** 102104

[21] Chen Z Y, Yuan H T, Wang X Q, Ma N, Zhang Y W, Shimotani H, Qin Z X, Shen B and Iwasa Y 2013 *Appl. Phys. Lett.* **103** 253508

[22] Cronin S B, Barnett R, Tinkham M, Chou S G, Rabin O, Dresselhaus M S, Swan A K, Ünlü M S and Goldberg B B 2004 *Appl. Phys. Lett.* **84** 2052

[23] Das A, Pisana S, Chakraborty B, Piscanec S, Saha S K, Waghmare U V, Novoselov K S, Krishnamurthy H R, Geim A K, Ferrari A C and Sood A K 2008 *Nat. Nanotechnol.* **3** 210

[24] Abstreiter G, Claessen U and Tränkle G 1982 *Solid State Commun.* **44** 673

[25] Abstreiter G, Huber R, Tränkle G and Vinter B 1983 *Solid State Commun.* **47** 651

[26] Miller N, Ager III J W, Smith III H M, Mayer M A, Yu K M, Haller E E, Walukiewicz W, Schaff W J, Gallinat C, Koblmüller G and Speck J S 2010 *J. Appl. Phys.* **107** 113712

[27] Wang K, Miller N, Iwamoto R, Yamaguchi T, Mayer M A, Araki T, Nanishi Y, Yu K M, Haller E E, Walukiewicz W and Ager J W 2011 *Appl. Phys. Lett.* **98** 42104

[28] Yeo B S, Klaus S L, Ross P N, Mathies R A and Bell A T 2010 *ChemPhysChem* **11** 1854

[29] Ager J W, Miller N, Jones R E, Yu K M, Wu J, Schaff W J and Walukiewicz W 2008 *Phys. status solidi* **245** 873

[30] Brown G F, Ager J W, III, Walukiewicz W, Schaff W J and Wu J 2008 *Appl. Phys. Lett.* **93** 262105

[31] Khanal D R, Walukiewicz W, Grandal J, Calleja E and Wu J 2009 *Appl. Phys. Lett.* **95** 173114

[32] Lu H, Schaff W J, Eastman L F and Stutz C E 2003 *Appl. Phys. Lett.* **82** 1736

[33] Inushima T, Higashiwaki M and Matsui T 2003 *Phys. Rev. B* **68** 235204

[34] Wang X, Che S-B, Ishitani Y and Yoshikawa A 2006 *Appl. Phys. Lett.* **89** 171907

[35] Bungaro C, Rapcewicz K and Bernholc J 2000 *Phys. Rev. B* **61** 6720

[36] Berggren K and Sernelius B 1981 *Phys. Rev. B* **24** 1971

[37] Das Sarma S, Jalabert R and Yang S-R E 1989 *Phys. Rev. B* **39** 5516

[38] Jalabert R and Das Sarma S 1989 *Phys. Rev. B* **40** 9723

[39] King P D C, Veal T D, McConville C F, Zúñiga-Pérez J, Muñoz-Sanjosé V, Hopkinson M, Rienks E D L, Jensen M F and Hofmann P 2010 *Phys. Rev. Lett.* **104** 256803

[40] Tränkle G, Leier H, Forchel A, Haug H, Ell C and Weimann G 1987 *Phys. Rev. Lett.* **58** 419

[41] Kane E O 1957 *J. Phys. Chem. Solids* **1** 249

[42] Chuang S and Chang C 1996 *Phys. Rev. B* **54** 2491

[43] Wu J 2009 *J. Appl. Phys.* **106** 11101

[44] Chang Y-M, Chu H W, Shen C-H and Gwo S 2007 *Appl. Phys. Lett.* **90** 72110

[45] Pomeroy J W, Kuball M, Swartz C H, Myers T H, Lu H and Schaff W J 2007 *Phys. Rev. B* **75** 35205

[46] Schäfer-Nolte E O, Stoica T, Gotschke T, Limbach F A, Sutter E, Sutter P, Grützmacher D and Calarco R 2010 *Nanotechnology* **21** 315702

[47] Jeganathan K, Purushothaman V, Debnath R K, Calarco R and Luth H 2010 *Appl. Phys. Lett.* **97** 93104

[48] Sahoo S, Hu M S, Hsu C W, Wu C T, Chen K H, Chen L C, Arora A K and Dhara S 2008 *Appl. Phys. Lett.* **93** 233116

[49] Zhu J H, Ning J Q, Zheng C C, Xu S J, Zhang S M and Yang H 2011 *Appl. Phys. Lett.* **99** 113115